

Impact of cumulus cloud spacing on Landsat atmospheric correction and aerosol retrieval

Guoyong Wen

Joint Center for Earth Systems Technology, University of Maryland Baltimore County, Catonsville, Maryland
NASA Goddard Space Flight Center, Greenbelt, Maryland

Robert F. Cahalan and Si-Chee Tsay

NASA Goddard Space Flight Center, Greenbelt, Maryland

Lazaros Oreopoulos

Joint Center for Earth Systems Technology, University of Maryland Baltimore County, Catonsville, Maryland
NASA Goddard Space Flight Center, Greenbelt, Maryland

Abstract. A Landsat 7 Enhanced Thematic Mapper Plus (ETM+) image acquired over the Southern Great Plains site of Department of Energy's Atmospheric Radiation Measurement Program during the Atmospheric Radiation Measurement Enhanced Shortwave Experiment II is used to study the effect of clouds on reflected radiation in clear gaps in a cumulus cloud field. A technique using the spectral information of background and clouds is applied to identify clouds. The path radiance technique is used to extract the apparent path radiance in a clear region of the cumulus cloud field. The result shows that the apparent path radiance is enhanced by nearby clouds in both band 1 (blue) and band 3 (red) of ETM+. More importantly, the magnitude of the enhancement depends on the mean cloud-free distance in the clear patches. For cloud-free distances < 0.5 km the enhancement of apparent path radiance is more than 0.025 and 0.015 (reflectance units) in band 1 and band 3, respectively, which corresponds to an enhancement of apparent aerosol optical thickness of ~ 0.25 and ~ 0.15 . Neglecting of the three-dimensional cloud effect would lead to underestimates of surface reflectance of ~ 0.025 and ~ 0.015 in the blue and red band, respectively, if the true aerosol optical thickness is 0.2 and the surface reflectance is 0.05. The enhancement decreases exponentially with mean cloud-free distance, reaching asymptotic values of 0.09 for band 1 and 0.027 for band 3 at a mean cloud-free distance about 2 km. The asymptotic values are slightly larger than the mean path radiances retrieved from a completely clear region: 0.086 and 0.024 for the blue and red bands, respectively.

1. Introduction

Modern era Earth observations from satellite platforms provide a good opportunity to sense remotely surface reflective characteristics and atmospheric properties on a global scale. Techniques have been developed to retrieve aerosol optical thicknesses and to correct atmospheric effects for satellite images in clear-sky conditions [Kaufman *et al.*, 1997; Wen *et al.*, 1999]. In a clear atmosphere, solar radiative transfer may be described accurately by a plane parallel approach [Stamnes *et al.*, 1988; Tsay *et al.*, 1990]. However, the global average cloud cover is about 60%, so that satellite images in many geographic locations are often contaminated with clouds. Excluding cloudy scenes not only limits the usefulness of satellite measurements but also leads to clear-sky biases in retrieved atmospheric properties since much of the clear-sky near clouds is excluded.

One cloud type with interesting properties that appears frequently in satellite images is fair weather cumulus. Landsat

measurements have been used to investigate the statistics of cumulus cloud fields [Wielicki and Welch, 1986; Cahalan and Joseph, 1989; Joseph and Cahalan, 1990]. High spatial resolution Landsat images are also useful for studying radiative transfer in clear patches of cumulus cloud fields. Surface features in clear patches are apparent in satellite images just by visual inspection, indicating a major contribution from the clear region itself. Therefore it is possible to infer surface reflective characteristics and atmospheric properties even in the presence of scattered cumulus when satellite spatial resolution is sufficient to resolve cloud-free gaps.

Compared with the path radiance in a completely clear region, Cahalan *et al.* [2001] found that the apparent path radiance of Enhanced Thematic Mapper Plus (ETM+) band 1 at $0.49 \mu\text{m}$ and band 3 at $0.66 \mu\text{m}$ for clear patches in a cumulus cloud field was significantly enhanced by nearby clouds, leading to an overestimate of aerosol optical thickness and, consequently, to an underestimate of surface reflectance. However, quantifying this effect and linking it to cumulus cloud characteristics is a great challenge because of the complex nature of cumulus clouds.

Despite cloud complexity several fundamental questions can be addressed in studying the cloud effects on radiation in clear

Copyright 2001 by the American Geophysical Union.

Paper number 2001JD900159.
0148-0227/01/2001JD900159\$09.00

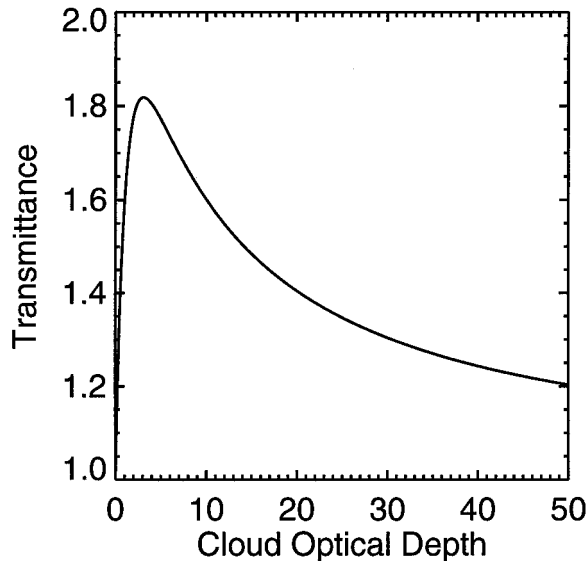


Figure 1. Transmittance at the surface level underneath a small clear hole in a plane parallel cloud as a function of cloud optical depth for overhead Sun. DISORT with a C.1 cloud is used to calculate the diffuse radiation. Atmospheric effects are ignored.

regions of cumulus fields. First, we would like to know to what extent clouds affect radiation in nearby clear regions. Second, we want to examine how to quantify cloud effects by looking for major factors responsible for these effects. For example, cloud effects are expected to be less pronounced when clouds are separated farther apart. Can this phenomenon be observed? Can we parameterize cloud effects in satellite images? In section 2 we present theoretical results to demonstrate the potential extent of cloud effects on downwelling irradiance at the surface. In sections 3 and 4 we describe the data set and analysis technique. In section 5 we show the dependence of path radiance on cloud-free distance, the resulting impact on aerosol and surface retrievals, and how such retrievals can be corrected for cloud effects.

2. Preliminaries

Cumulus clouds have a complex geometry, as we see from satellite images or our day-to-day experience. Research has shown the fractal structure of cumulus cloud fields [Cahalan and Joseph, 1989]. The description of radiative transfer in cumulus cloud fields requires a solution of the radiative transfer equation in three-dimensional (3-D) space. Because of the complicated nature of cumulus clouds, a full description of radiative transfer as a function of cloud optical properties in a realistic, spatially extensive cumulus cloud field is not feasible at the present time. However, we may still be able to examine the extent of influence of clouds on nearby clear regions without complicated 3-D radiative transfer calculations.

Clouds can either reduce or enhance solar radiation locally. Cumulus clouds reflect solar radiation away, casting shadows at the ground. This shadowing effect reduces solar radiation at the surface. The multiple scattering of sunlight in cumulus clouds increases diffuse radiation, enhancing the downwelling solar flux at the surface level. This phenomenon has been observed by ground level radiometers [e.g., Mims and Frederick, 1994].

For simplicity we shall examine the extent of cloud effects on the downwelling irradiance at the surface level. It is evident that the shadowing effects reach maximum when the cloud has infinitely large optical depth with sufficiently large horizontal dimensions. In this case the surface irradiance approaches zero.

To demonstrate the magnitude to which clouds could potentially enhance the downwelling irradiance at the surface level in a clear region, we examine an idealized situation of a “hole” or clear patch in a plane parallel cloud with an overhead Sun. The hole is assumed to be small but large enough to contain the solar disk for surface viewers directly below (the solar disk is about a half degree viewed from the Earth). For simplicity, atmospheric effects (aerosol, molecular scattering, and absorption) are ignored, and surface reflectance is assumed to be zero. (An example that may approximate this simplified cloud is a Karman vortex cloud over ocean, similar to the one recently discussed by DeFelice *et al.* [2000].)

The downwelling irradiance in the clear hole at the surface level is the sum of the irradiance directly through the hole (F_0) and the diffuse radiation from cloud (F_d). Since the hole is assumed to be very small, the downwelling diffuse irradiance from the cloud may be approximated by that from a plane parallel cloud. The total transmittance of the solar irradiance at the surface underneath the clear hole may be defined as

$$T = \frac{F_0 + F_d}{F_0}. \quad (1)$$

Since the atmospheric effects are ignored, F_0 is the same as the solar irradiance at the top of the atmosphere. The diffuse component is calculated using the discrete ordinates radiative transfer model (DISORT) [Stamnes *et al.*, 1988; Tsay *et al.*, 1990] with the conservative scattering C.1 phase function [Deirmendjian, 1969].

The transmittance through the clear hole at the surface level is presented as a function of cloud optical depth (Figure 1). It is evident that the total downwelling irradiance at the surface level increases quickly with cloud optical depth, reaching a maximum of about 1.82 times that of purely clear sky at a cloud optical depth of 3, then decreasing monotonically as cloud optical depth increases.

Even though this example is highly simplified, it reveals that the basic physical mechanism of cloud effects on the irradiance in clear gaps is through the diffuse radiation generated by multiple scattering of sunlight in clouds. Though an 82% increase in downwelling irradiance is a theoretical upper bound for this idealized model, it implies that the enhancement of solar radiation in clear regions of a cloudy atmosphere due to cloud adjacency effects is potentially large. Furthermore, if there is an aerosol layer underneath the cloud, and/or the surface is nonblack, the additional diffuse radiation from clouds impinging on aerosols and the surface can greatly enhance the reflected solar radiation at the top of the atmosphere. If cloud adjacency effects are not accounted for, the satellite observed solar radiances will be misinterpreted, leading to large errors in the aerosol optical thickness and surface reflectance retrievals.

In real cumulus cloud fields, optically dense clouds with fractal properties embedded in an optically thin atmosphere consisting of molecules and aerosols make the effects much more complicated and interesting [Cahalan *et al.*, 2001]. The cloud side effects might dominate the enhancement in a clear region nearby. In the following sections we show that such

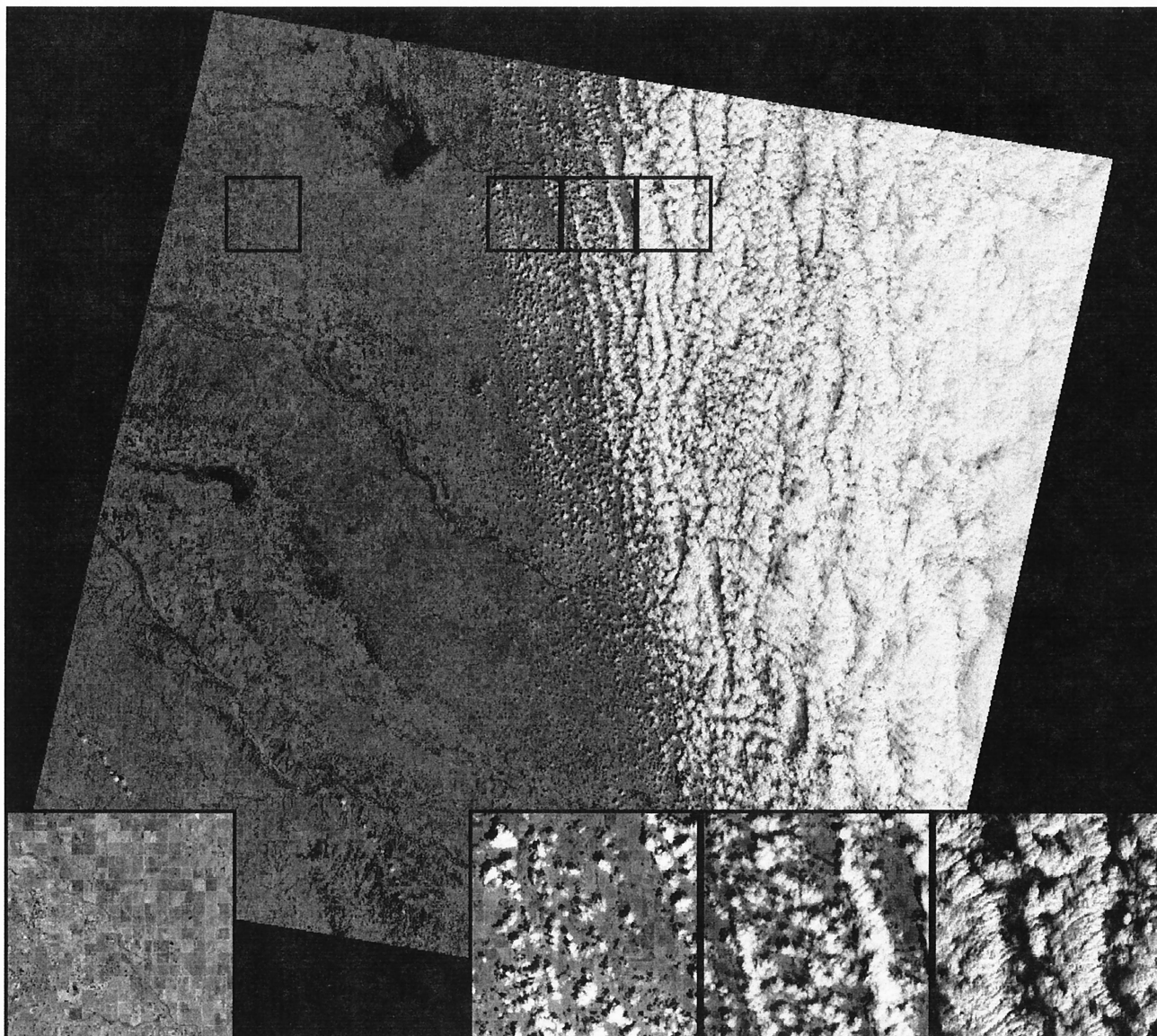


Figure 2. An ETM+ image acquired at 1700 UTC on March 19, 2000, over the SGP ARM site in Oklahoma. Blowups of subimages show details, with a completely clear subimage at the left and three consecutive subimages with increasing cloud cover toward the right.

cloud effects are observable and demonstrate that cloud spacing modulates the solar radiation reflected from clear regions of cumulus cloud fields observed by the Landsat 7 radiometer.

3. Data Description

The Landsat 7 satellite was launched on April 15, 1999, into a Sun synchronous orbit at an altitude of 705 km. The launch of Landsat 7 continues the long-term acquisition of high spatial resolution images on global scales. Similar to its predecessor Thematic Mapper (TM) on Landsat 4 and 5, the ETM+ on Landsat 7 has visible (bands 1, 2, and 3), near IR (band 4), and mid-IR (bands 5 and 7) bands at 30 m spatial resolution and a thermal infrared band at $11\ \mu\text{m}$ with 60 m resolution (band 6). In addition, the ETM+ has a new panchromatic band (band 8 at $0.52\text{--}0.9\ \mu\text{m}$) with a spatial resolution of 15 m. The improved ETM+ instrument has the ability to switch between

high- and low-gain settings. The thermal band has both high- and low-gain settings operating at the same time.

A Landsat 7 ETM+ scene centered at 36.04°N , 97.87°W was acquired at 1700 UTC on March 19, 2000, over the Oklahoma Southern Great Plains (SGP) site of Department of Energy's Atmospheric Radiation Measurement Program (DoE's ARM) during Atmospheric Radiation Measurement Enhanced Shortwave Experiment II (ARESE II) period. The solar zenith angle is 43° . The cloud cover of the $185\ \text{km} \times 180\ \text{km}$ ETM+ scene is about 40%, as shown in Figure 2. The four black areas outside the ETM+ image are filled with zeros to make the whole picture rectangular. The left portion of the scene is clear with a few small isolated cumuli. An overcast stratocumulus cloud can be seen at the right part of the image. From clear to overcast we see scattered fair weather cumulus clouds and cloud streets. As cloud cover increases from clear to overcast, the cloud spacing gradually decreases. Blowups of subimages

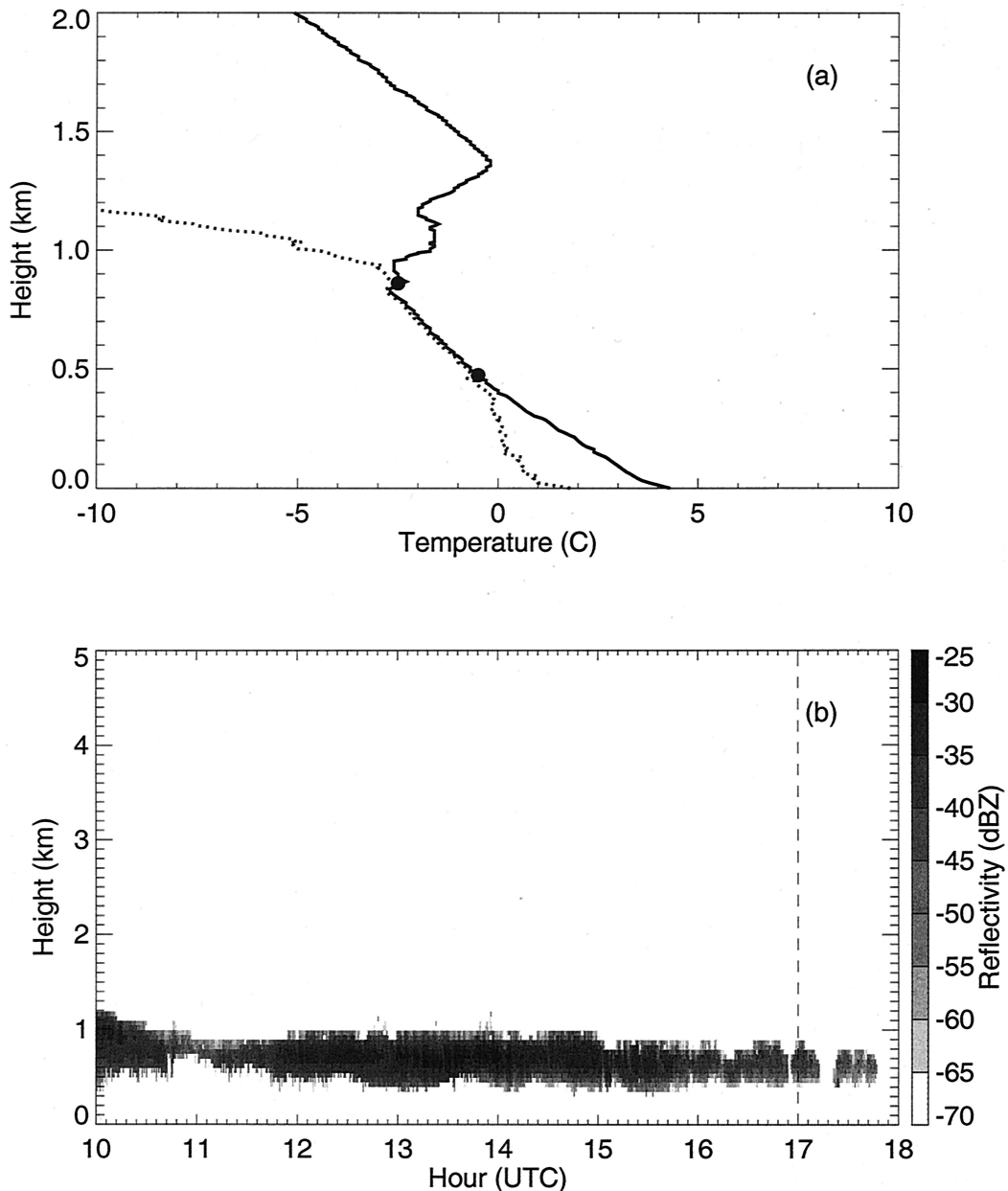


Figure 3. (a) The temperature (solid) and dew point temperature (dotted) profiles \sim 1430 UTC on March 19, 2000, over the ARM SGP site. The cloud base (\sim 473 m) and top (\sim 860 m) above the ground are indicated by solid circles. (b) The time series of MMCR reflectivity profile above the ground at the SGP ARM site indicates cloud base and top at about 0.5 and 1 km, respectively. The timing of a Landsat 7 overpass at 1700 UTC is indicated by a dashed vertical line.

of 512×512 pixels ($15 \text{ km} \times 15 \text{ km}$) from a completely clear region and three consecutive cloudy images at the bottom show details of cloud structure.

During ARESE II the Balloon-Borne Sounding System (BBSS) [Lesht, 1995] was launched from the central facility site at 36.6°N , 97.5°W (about 15 km east of the rightmost subimage in Figure 2) every 3 hours, taking vertical profile measurements of the thermodynamic state of the atmosphere and wind speed. The Millimeter-Wavelength Cloud Radar (MMCR) [Clothiaux *et al.*, 2000] and Belfort Laser Ceilometer (BLC) [Turner, 1996] located at the central facility site were operating continuously to measure cloud reflectivity and to detect the cloud base.

After examining the temperature and humidity profiles (not shown) of the balloon launched at 1728 UTC, 28 min after the Landsat 7 overpass, we concluded that it did not pass through clouds. However, prior temperature and humidity profiles at 1130 (not shown here) and 1430 UTC (Figure 3a) indicate the cloud base at 475 and 473 m and a cloud top height of 1015 and 860 m above the ground, respectively. The cloud base heights determined from the temperature and humidity are consistent with those from BLC (not shown). The MMCR reflectivity profile also indicates the cloud base at \sim 0.5 km and the cloud top at \sim 1 km above ground (Figure 3b). Gaps in the MMCR reflectivity profile before and after the Landsat 7 overpass indicate the

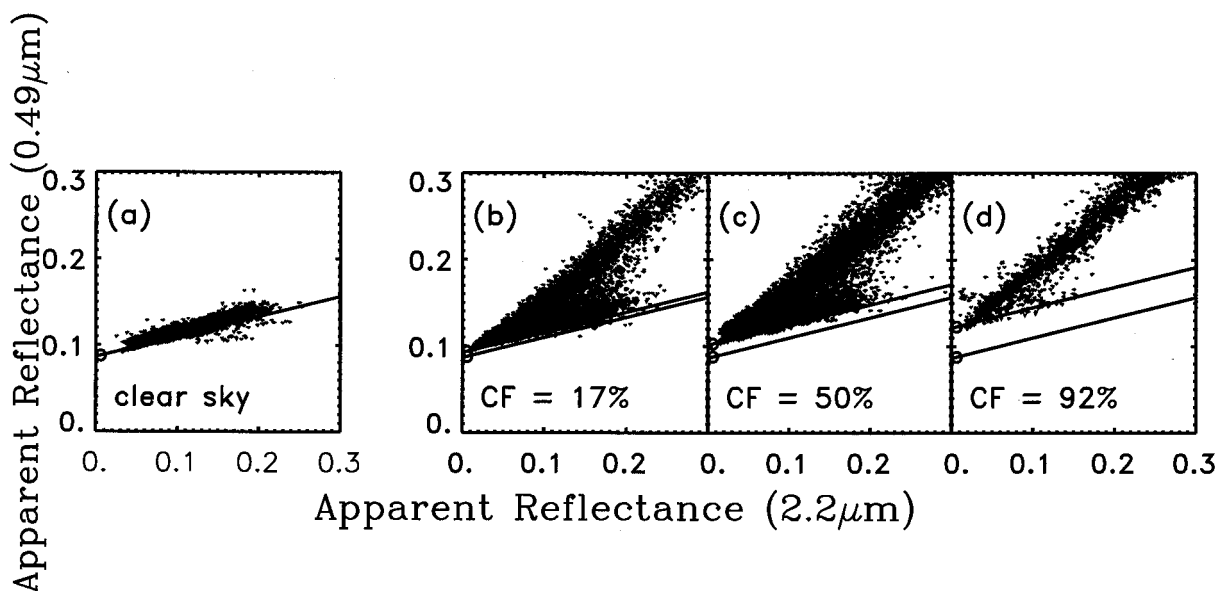


Figure 4. The relation between the visible at $0.49 \mu\text{m}$ (band 1) and the mid-IR band at $2.2 \mu\text{m}$ (band 7) for the four subimages in Figure 2: (a) clear sky and (b)–(d) cloudy subimages with different cloud fraction (CF) indicated. The intercept of zero mid-IR reflectance of a straight line that fits through the lower envelope of the visible and mid-IR relations determines the path radiance (for completely clear sky) and apparent path radiance (for clear patches in cumulus cloud field), respectively. The straight line used to determine the path radiance for clear sky (Figure 4a) is also plotted in cloudy cases (Figures 4b–4d) as a reference (lower lines).

clear region of cumulus cloud field passing over the central facility site.

We should note that the in situ profiles from the sounding and the ground-based MMCR and BCL remote measurements were made at a specific location in the $185 \text{ km} \times 180 \text{ km}$ ETM+ image. Together with the in situ measurements from BBSS, the continuous measurements from MMCR and BLC indicate that clouds observed from ETM+ have a cloud base about 0.5 km and cloud top height about 1 km above the ground. In this study we focus on the cumulus cloud field between the clear region and the stratocumulus (Figure 2).

4. Data Analysis

Cumulus cloud fields are complex in nature. Except for cloud shadows evident in high spatial resolution images the effects of clouds on reflected solar radiation in clear patches are not obvious. Even if the cloud effects can be identified, it may, nevertheless, be difficult to identify the major characteristics of cumulus clouds that cause these effects. In this section we review the path radiance method, discuss identification of clouds and cloud shadows, and describe how to extract information on cloud effects from ETM+ images and the characterization of cumulus cloud fields.

4.1. Apparent Path Radiance

The reflected solar radiance at each pixel of an ETM+ image depends not only on the optical properties of each individual cloud but also on how they are distributed in space. The complicated cloud geometric shape and spatial distribution make it very difficult to establish a one-to-one relationship between clear-sky radiance and the configuration of nearby clouds. The variable surface reflectance characteristics of land add another difficulty in assessing the cloud effects. Therefore

it is not straightforward to isolate cloud effects from a single band of ETM+ on a pixel-to-pixel basis.

The path radiance technique is proposed by *Wen et al.* [1999] to extract the atmospheric path radiance for the purpose of atmospheric correction and aerosol optical thickness retrieval. The path radiance technique uses two empirical observations: (1) aerosols have negligible effects in the $2.2 \mu\text{m}$ mid-IR band 7 of TM and ETM+, so the path radiance in band 7 is approximately zero, and (2) surface reflectance over vegetation and wet soil in bands 1 and 3 is linearly correlated to that in band 7 [*Kaufman et al.*, 1997]. Because most aerosol layers are optically thin, (2) implies that top-of-atmosphere reflectances in visible and mid-IR are also linearly correlated [*Wen et al.*, 1999]. The key step of this method is to extrapolate the visible–mid-IR linear relation of the top-of-atmosphere reflectance to zero reflectance in band 7, which corresponds to zero surface reflectance. The intercept then gives the atmospheric path radiance in the visible band as shown in Figure 4a for clear-sky conditions.

In an analysis of an ETM+ imagery, *Cahalan et al.* [2001] found that the visible and mid-IR observed reflectances are also linearly correlated in the clear gaps between cumulus clouds. Similar to the process for the clear atmosphere, *Cahalan et al.* [2001] fitted a straight line through the lower envelope of the visible and mid-IR relations for clear patch pixels within cumulus cloud fields. The intercept of the straight line at the zero of mid-IR reflectance, which would be close to the true path radiance if the atmosphere was completely clear, was found to be enhanced significantly compared to that of an entirely clear region. Since the satellite-observed solar radiation is affected by nearby clouds, the intercept no longer represents the true path radiance of the clear atmosphere. The intercept therefore is defined as “apparent path radiance.” Here we further demonstrate that the magnitude of the en-

hancement in apparent path radiance is affected by cloud spacing in the cumulus cloud field.

The visible (band 1 of ETM+) and mid-IR (band 7 of ETM+) observed reflectance relations for three subimages (Figure 2) of 512×512 pixels (or $\sim 15 \text{ km} \times 15 \text{ km}$) from the cloudy eastward side of the image are presented in Figure 4 along with those from a completely clear subimage on the westward side. It is evident that the lower envelope of the visible and mid-IR scattered points extracted from clear regions embedded in cloudy scenes is generally higher than the completely clear subimage as indicated by the lower straight line. The apparent path radiance determined from the intercept of zero of mid-IR of a straight line that fits through the lower envelope of the scattered relation for clear patches in cloudy region is evidently enhanced compared to the completely clear atmosphere.

The enhancement of apparent path radiance increases as cloud cover increases (or cloud spacing decreases). The enhancement of the apparent path radiance is 0.005 for the least cloudy subimage and 0.03 for the most cloudy subimage. These enhancements of visible reflectance are significant. An enhancement of the path radiance of about 0.005 and 0.03 will lead to an overestimate of aerosol optical thickness of 0.05 and 0.3, respectively, if a plane parallel atmosphere is assumed [Wen *et al.*, 1999]. An overestimate of aerosol optical thickness of 0.05 and 0.3 further leads to an underestimate of surface reflectance of about 0.005 and 0.03, respectively, if the true aerosol optical thickness is 0.2 with a surface reflectance of 0.05.

The apparent path radiance introduced here avoids the difficulty of assessing the cloud effect on the reflected solar radiation for individual pixels. Instead, it gives the statistics of the cloud effects relative to the plane parallel atmosphere. The apparent path radiance in clear patches of cumulus cloud fields is physically intuitive and can be measured and compared with the path radiance in completely cloud-free regions of the same image, thus allowing determination of the impact of scattered cumulus clouds on apparent path radiance. In section 5 we present details of how cloud spacing affects the apparent path radiance.

4.2. Cloud Mask

Figure 4 showed that the enhancement of the apparent path radiance depends on cloud spacing in the cumulus field. Before we can further discuss cloud spacing effects on the reflected solar radiation we need to have an accurate cloud identification scheme. A variety of techniques has been developed to identify clouds for satellite images [Coakley and Bretherton, 1982; Ackerman *et al.*, 1998]. Landsat 7 uses the Automated Cloud Cover Assessment (ACCA) algorithm [Irish, 2000] for its acquisition strategy, but in our study, there is no need to use such a complex technique. Instead, we use simple spectral discrimination to separate cloud from vegetation and bare soil background.

The reflectance of vegetation and soil depends strongly on wavelength in the solar spectrum, i.e., small in visible and large in near-IR [Short, 1982], while the reflectance of clouds has less preferential dependence in those wavelengths. This is particularly true for opaque clouds (i.e., cumulus, stratocumulus, and stratus clouds). We found two bands are sufficient to identify clouds for the Oklahoma scene where surface is mostly vegetated or bare soil. A visible (band 2 at $0.57 \mu\text{m}$) and a near-IR band (band 4 at $0.84 \mu\text{m}$) are used for cloud masking.

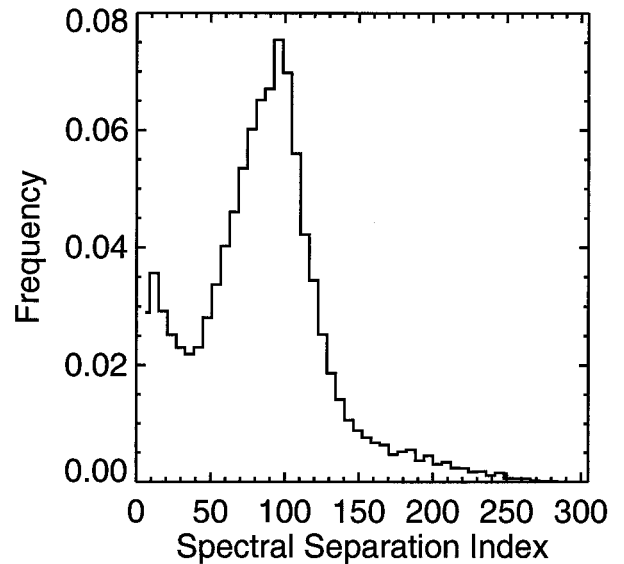


Figure 5. The SSI for a subimage of Figure 6 is characterized by a bimodal distribution. The mode with smaller SSI comes from cloud pixels. The clear pixels form the mode on the right. The long tail at right comes from shadow pixels. A threshold value of 40, defined by the minimum between peaks, is used to separate cloudy from clear pixels, and 150 is used as a cutoff for shadow pixels.

To use the spectral information, we define a unit vector composed from the reflectance of two bands:

$$\mathbf{P} = \frac{(r_2, r_4)}{\sqrt{r_2^2 + r_4^2}}, \quad (2)$$

where r_2 and r_4 are observed reflectances of bands 2 and 4 of ETM+. A normalized spectral separation index (SSI) is defined to identify clouds:

$$Q = \frac{\mathbf{P} \cdot \mathbf{I}}{r_2} \quad (3)$$

$$\mathbf{I} = \left(\frac{1}{\sqrt{2}}, \frac{1}{\sqrt{2}} \right)^T, \quad (4)$$

where \mathbf{I} is a unit vector in the 2-D reflectance space. The dot product $\mathbf{P} \cdot \mathbf{I}$ measures the degree of wavelength independence of reflectance at the two bands. It ranges from 0 to 1 and takes values close to 1 when reflectances in the two bands are about equal, as for clouds. Since the surface reflectance of visible band over vegetation and bare soil is small, and cloud reflectance is relatively large for both visible and near-IR bands, the weighting factor of visible reflectance r_2 in the denominator of (3) makes the index Q effective in separating clear from cloudy pixels.

A subimage of 512×512 pixels is used to demonstrate the cloud-masking process. The histogram of the Q index of the subimage (Figure 5) clearly shows a bimodal distribution. The value of Q corresponding to the minimum between the two modes ($Q_0 \sim 40$) can be used as a threshold to separate cloudy from clear pixels. Pixels with $Q < Q_0$ are classified as cloudy or clear otherwise.

The distribution of Q is positively skewed with a long tail toward large values. Pixels in the right tail can be shown to

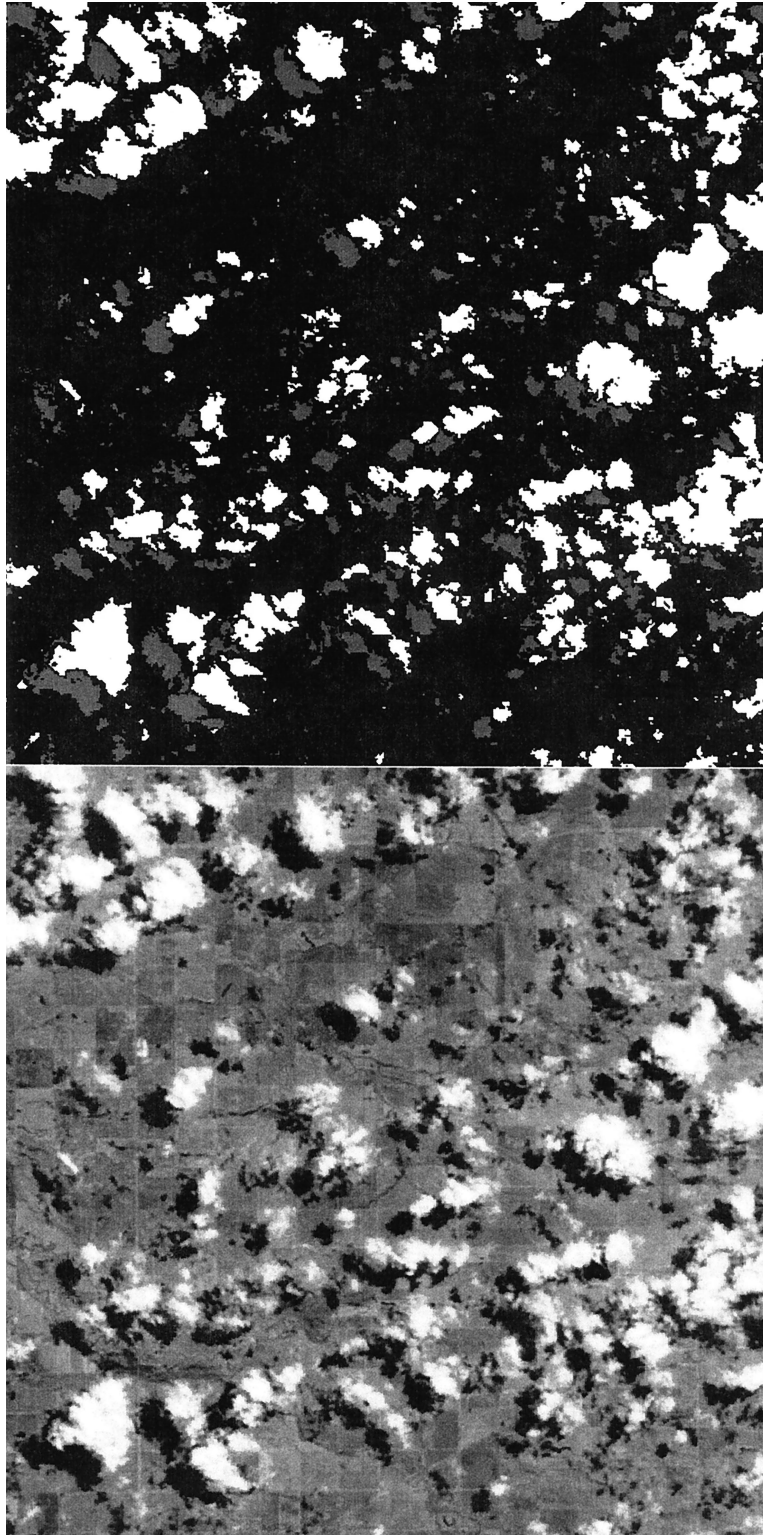


Figure 6. (right) The cloud shadow mask using the SSI technique is compared with (left) the original image.

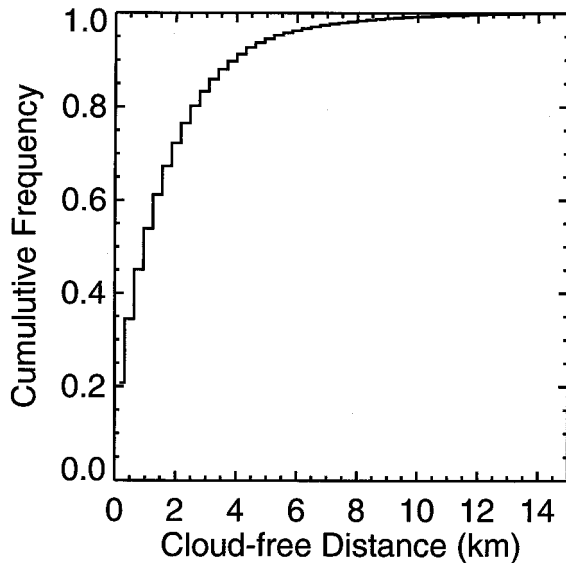


Figure 7. The cumulative distribution of cloud-free distance for clear regions in the cumulus cloud field for the subimages in Figure 6.

come mainly from cloud shadows. That is because the reflectance is wavelength-dependent over shadows and the denominator in (3) is smaller for shadows than for nonshadow pixels. Therefore the spectral separation index Q is expected to be larger for shadow pixels relative to nonshadow clear pixels.

Unlike a clear bimodal distribution for clear and cloudy pixels, there is no clear cutoff for the shadows. We found that a threshold value of 150 is an appropriate cutoff value by visual examination of the shadow mask and the original image. The shadow mask is not very sensitive to the threshold value chosen. Some shadow pixels near the big cloud street are misclassified, but most clouds and shadows are captured, as can be seen in Figure 6.

4.3. Cloud-Free Distance

Strictly speaking, the radiance at each individual clear pixel in a 2-D image depends on the distribution of cloud and aerosol optical properties in 3-D space, as well as surface reflectance. In section 4.1 we mentioned that the evaluation of the effects of cloud on reflected solar radiation on a pixel-by-pixel basis is not practical because of the complicated nature of clouds and surface reflectance. A measurable parameter, the apparent path radiance, was introduced to quantify the cloud effects. To understand better the cloud effects physically, we now explore further the major causes of these effects.

What is needed is a parameter describing the primary statistical property of cumulus cloud fields that affects surface illumination, rather than detailed information on individual cumulus clouds. By visually inspecting the apparent path radiance and associated image we found that the apparent path radiance depends primarily on cloud spacing. This is physically intuitive since the farther away the cloud is, the weaker the diffuse radiation from the cloud, and thus the smaller the effects.

For ideal bar clouds, or lattice cuboid clouds, the distance (edge to edge) between two clouds can be used to describe cloud spacing. In a real cumulus cloud field this definition of cloud spacing is not useful. The geometry of cumulus clouds

has a fractal structure [Cahalan and Joseph, 1989] with the probability distribution of cloud areas approximately following a power law [Wielicki and Welch, 1986; Cahalan and Joseph, 1989]. Because of the nature of a power law distribution (i.e., large number of smaller clouds), the conventional edge-to-edge cloud spacing primarily represents the distance among the smaller clouds and is thus not suitable for our purposes.

Even though cumulus cloud fields are quite complicated, they still have some special features that can be used to characterize their influence on apparent path radiance. Except for cumulus congestus, cumulus clouds have nearly flat bases at the lifting condensation level, with fairly small protuberances at the top [Cotton and Anthes, 1989]. So, cloud altitude and thickness are not greatly variable in the ETM+ image. This is consistent with the in situ and ground-based measurements of clouds in this study shown earlier. Aerosol properties are also often uniform over the scale of a Landsat ETM+ image ($\sim 185 \text{ km} \times 180 \text{ km}$). Therefore we primarily need a parameter that describes the cloud spacing in a 2-D field.

Since we are mainly interested in the radiation in clear patches, and the effects from nearby clouds, it is natural to link the two (i.e., to examine the statistics of distance between a clear pixel and a nearby cloud). In this study we define the cloud-free distance of a clear pixel as the distance from the clear pixel to the closest cloud along the principal plane. The rationale for choosing the principal plane is that the sunlit parts of cumulus clouds are generally brilliant white; hence this side has the largest contribution to sunlight reflected onto the nearby surface and aerosols.

The cumulative distribution of cloud-free distances for the least cloudy subimage is presented in Figure 7 as an example. The mean cloud-free distance of the subimage is 1.7 km, with a standard deviation 1.9 km. It is also interesting to note that as many as half of the clear pixels have cloud spacing $< 1 \text{ km}$, and only the top tenth percentile of the clear pixels has a cloud-free distance $> 4 \text{ km}$.

5. Dependence of Apparent Path Radiance on Cloud Spacing

Because the geometrical thickness of fair weather cumulus clouds is relatively constant and aerosol properties do not vary dramatically within Landsat ETM+ images in the remote rural region of the Oklahoma ARM site, the mean cloud-free distance is expected to be a major dependence variable of cloud effects. Here we study explicitly the relation between the observed apparent path radiance and the mean cloud-free distance.

In the analysis process we calculated both the mean cloud-free distance and the apparent path radiance in a cloudy subimage of 512×512 pixels ($\sim 15 \text{ km} \times 15 \text{ km}$). The choice of the size of the subimage takes into consideration that the size should be much larger than typical cumulus clouds, i.e., $< 1 \sim 2 \text{ km}$ from the power law distribution [Cahalan and Joseph, 1989]. The size should be also small enough to allow us to examine the apparent path radiance in different regions within the cumulus cloud field. In order to increase statistical significance a moving window of 512×512 pixels at an increment of 200 pixels both in the horizontal and vertical is applied. Since we are interested in examining the effects of cloud on radiances of clear patches, the amount of both clear and cloud pixels should be significant in any subimage. We therefore excluded subimages with cloud cover $< 2\%$ or $> 85\%$.

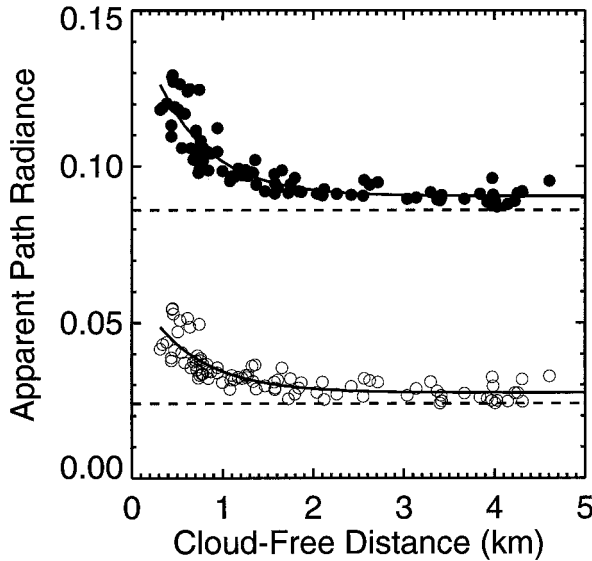


Figure 8. The apparent path radiance for ETM+ band 1 (solid circles) and band 3 (open circles) as a function of mean cloud-free distance, defined in the text.

The mean cloud-free distance and apparent path radiance for both band 1 and band 3 are plotted in Figure 8. Each point in Figure 8 represents the mean cloud-free distance and corresponding apparent path radiance of a subimage. The average path radiance from the clear atmosphere far away from clouds is used as a reference and plotted with a dashed line.

It is evident that the apparent path radiance is enhanced in the cumulus cloud field. The enhancement in the blue band is generally larger than that in the red band. The enhancement and associated variability increase as the mean cloud-free distance decreases for both visible bands and exceeds 0.025 and 0.015 for band 1 and band 3, respectively, when the mean cloud-free distance is <0.5 km. The enhancement decreases to an asymptotic value at a mean cloud-free distance of about 2 km. An analytical form of exponential decrease is used to parameterize the apparent path radiance and cloud-free distance relationship. The nonlinear best fits for blue and red bands are

$$r_{0.49\mu\text{m}} = 0.061e^{-x/0.586} + 0.090 \quad (5)$$

$$r_{0.66\mu\text{m}} = 0.035e^{-x/0.611} + 0.027, \quad (6)$$

where x is the mean cloud-free distance in kilometers.

The path radiance in the clear atmosphere away from clouds for band 1 and band 3 is presented in Figure 9 to examine the significance of the enhancement. The path radiances are clustered for both blue and red bands except for several outliers. Means are 0.086 and 0.024 with standard deviation of 0.0023 and 0.0029 for band 1 and band 3, respectively, excluding the top and bottom fifth percentiles. With these small standard deviations the mean values of path radiance represent the true clear-sky path radiance for both bands.

By comparing the apparent path radiance with the true path radiance and its dispersion it is evident that the apparent path radiance is greatly enhanced for subimages with mean cloud-free distances <1 km. Enhancements of up to 0.025 for band 1 and 0.015 for band 3 lead to overestimates of aerosol optical thickness of 0.25 and 0.15 [Wen et al., 1999]. The overestimate

in aerosol optical thickness further leads to underestimates in surface reflectance. For example, if the true aerosol optical thickness is 0.2 with a surface reflectance of 0.05, the surface reflectance will be underestimated by 0.025 and 0.015 for the two bands [Wen et al., 1999]. Even with larger mean cloud-free distance, the asymptotic apparent path radiances are still systematically larger than the average true path radiance at about 1 standard deviation level.

6. Summary and Discussion

The downwelling irradiance of solar radiation in cloud-free regions at the surface may be greatly enhanced by diffuse radiation from nearby clouds. A simple radiative transfer calculation shows that the enhancement of irradiance in a clear region could reach more than 80% at the surface. The enhanced downwelling irradiance interacting with molecules and aerosols in the atmosphere and the surface ultimately increases the reflected solar radiation. Without considering such effects the satellite observed radiance might be misinterpreted.

Fair weather cumulus is a very common cloud type in the atmosphere. It is important to study the solar radiation transfer in clear patches of cumulus cloud fields for both atmospheric correction and aerosol optical property retrieval in high spatial resolution satellite images. Among other factors the reflected solar radiation is affected by the cloud spacing. In this paper we demonstrated that the cloud effects on reflected solar radiation in clear breaks within cumulus cloud fields can be observed and quantified using the apparent path radiance that depends on cloud spacing.

Cloud effects not only can be observed using the apparent reflectance but also can be parameterized by the cloud-free distance for clear pixels. Apparent path radiance is greatly enhanced when mean cloud-free distance becomes small. For

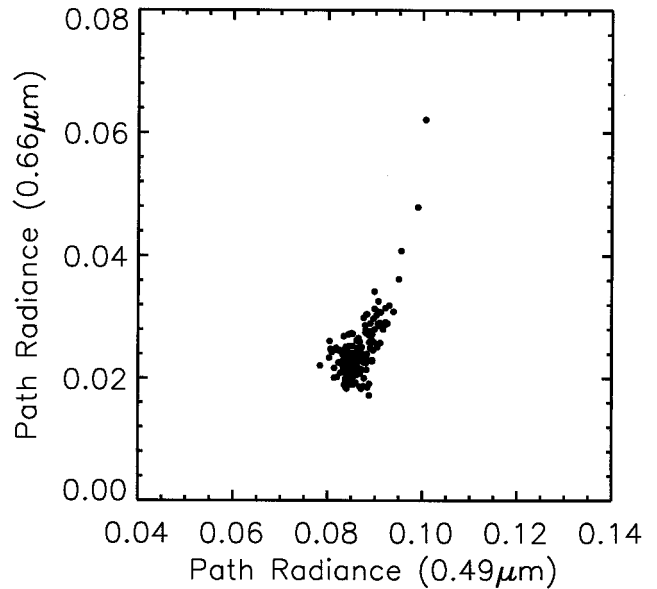


Figure 9. The path radiance for ETM+ band 1 and band 3 for clear regions away from cumulus cloud fields. The path radiances are clustered tightly for both bands except for several outliers. The means of the path radiances are 0.086 and 0.024, with standard deviations of 0.002 and 0.003 for band 1 and band 3, respectively, with top and bottom fifth percentiles excluded.

a subimage with mean cloud-free distance <0.5 km the apparent path radiances are enhanced by more than 0.025 and 0.015 for the blue band and the red band, respectively. These enhancements correspond to overestimates of aerosol optical thickness of ~ 0.25 and ~ 0.15 and underestimates of surface reflectance of ~ 0.025 and ~ 0.015 for the blue and red bands, respectively, for plane parallel retrievals. The enhancement of the apparent path radiance decreases exponentially with mean cloud-free distance. As the mean cloud-free distance becomes larger than 2 km, the apparent path radiance approaches asymptotically 0.09 and 0.027 for the blue and red bands, respectively. Even though the absolute difference between asymptotic values of apparent path radiance and the true path radiance is small, it is still statistically significant. However, it also indicates that only a constant correction is needed when cloud cells are far away from each other. We also need to note that values of asymptotic apparent path radiance apply only in the cloudy subimages with cloud cover $>2\%$ and $<85\%$.

The results and the technique used in this study are encouraging for further research in clear-cloudy interaction. However, they are based on an ETM+ image where the cumulus cloud appears to be uniform in vertical extent. The vertical thickness may vary from one cumulus cloud field to another (e.g., slight vertical extent for cumulus himilis and moderate vertical extent for cumulus mediocris) and hence the optical depth of clouds may vary. Cloud microphysics also affects the optical properties of cloud. Aerosol properties may vary from one cumulus cloud field to another. The solar zenith angle is an important parameter in radiative transfer of solar radiation and should be included in the parameterization. Further analysis of high spatial resolution images is needed to validate the parameterization in this study and to take into account other factors.

Acknowledgments. Data were obtained from the Atmospheric Radiation Measurement Program (ARM) sponsored by the Office of Science, Office of Biological and Environmental Research, Environmental Sciences Division, U.S. Department of Energy. This research was supported by funding provided under Landsat Science Team activities, which is part of NASA-MTPE, under proposal 1996-MTPE-00116 of the Department of Energy's ARM program under grant DE-A102-00ER62939. We thank C. Bohren and A. Marshak for stimulating discussions.

References

- Ackerman, S. A., K. I. Strabala, W. P. Menzel, R. A. Frey, C. C. Moeller, and L. E. Gumley, Discrimination clear sky from clouds with MODIS, *J. Geophys. Res.*, **103**, 32,141–32,157, 1998.
- Cahalan, R. F., and J. H. Joseph, Fractal statistics of cloud fields, *Mon. Weather Rev.*, **117**, 261–272, 1989.
- Cahalan, R. F., L. Oreopoulos, G. Wen, A. Marshak, S.-C. Tsay, and T. DeFelice, Cloud characterization and clear sky correction from Landsat 7, *Remote Sens. Environ.*, in press, 2001.
- Clouthiaux, E. E., T. P. Ackerman, G. G. Mace, K. P. Moran, R. T. Marchand, M. A. Miller, and B. E. Martner, Objective determination of cloud heights and radar reflectivities using a combination of active remote sensor at the ARM CART sites, *J. Appl. Meteorol.*, **39**, 645–665, 2000.
- Coakley, J. A., and F. P. Bretherton, Cloud cover from high-resolution scanner data: Detecting and allowing for partially filled fields of view, *J. Geophys. Res.*, **87**, 4917–4932, 1982.
- Cotton, W. R., and R. A. Anthes, *Storm and Cloud Dynamics*, Academic, San Diego, Calif., 1989.
- DeFelice, T. P., D. J. Meyer, G. Xian, J. Christopherson, and R. F. Cahalan, Landsat 7 reveals more than just surface features in remote area of globe, *Bull. Am. Meteorol. Soc.*, **81**, 1047–1049, 2000.
- Deirmendjian, D., *Electromagnetic Scattering on Spherical Polydispersions*, 291 pp., Elsevier Sci., New York, 1969.
- Irish, R., Landsat 7 automatic cloud cover assessment, in *Proceedings of SPIE/AeroSense, 2000: Algorithms for Multispectral, Hyperspectral, and Ultraspectral Imagery VI*, vol. 4049, pp. 348–355, Int. Soc. for Opt. Eng., Bellingham, Wash., 2000.
- Joseph, J. H., and R. F. Cahalan, Nearest-neighbor spacing of fair-weather cumulus, *J. Appl. Meteorol.*, **29**, 793–805, 1990.
- Kaufman, Y. J., A. E. Wald, L. A. Remer, B.-C. Gao, R.-R. Li, and L. Flynn, The MODIS 2.1- μm channel correlation with visible reflectance for use in remote sensing of aerosol, *IEEE Trans. Geosci. Remote Sens.*, **35**, 1286–1298, 1997.
- Lesht, B. M., An evaluation of ARM radiosonde operational performance, paper presented at Ninth Symposium on Meteorological Observations and Instrumentation, Am. Meteorol. Soc., Boston, Mass., 1995.
- Mims, F. M., and J. E. Frederick, Cumulus clouds and UV-B, *Nature*, **371**, 291, 1994.
- Short, N., The Landsat tutorial workbook, in *Basics of Satellite Remote Sensing, NASA Ref. Publ.*, vol. 1078, 553 pp., U.S. Gov. Print. Off., Washington D.C., 1982.
- Stamnes, K., S. C. Tsay, W. Wiscombe, and K. Jayaweera, Numerically stable algorithm for discrete-ordinate-method radiative transfer in multiple scattering and emitting layered media, *Appl. Opt.*, **27**, 2502–2509, 1988.
- Tsay, S.-C., K. Stamnes, and K. Jayaweera, Radiative transfer in stratified atmospheres: Development and verification of a unified model, *J. Quant. Spectrosc. Radiat. Transfer*, **43**, 133–148, 1990.
- Turner, D. D., Comparisons of the micropulse lidar and the Belfort Laser Ceilometer at the Atmospheric Radiation Measurement Southern Great Plains Cloud and Radiation Testbed Site, paper presented at Sixth Atmospheric Radiation Measurement (ARM) Science Team Meeting, San Antonio, Tex., 1996.
- Wen, G., S.-C. Tsay, R. F. Cahalan, and L. Oreopoulos, Path radiance technique for retrieving aerosol optical thickness over land, *J. Geophys. Res.*, **104**, 31,321–31,332, 1999.
- Wielicki, B. A., and R. M. Welch, Cumulus cloud properties derived using Landsat satellite data, *J. Clim. Appl. Meteorol.*, **25**, 261–276, 1986.
- R. F. Cahalan, L. Oreopoulos, S.-C. Tsay, and G. Wen, Climate and Radiation Branch; NASA/GSFC, Greenbelt, MD 20771. (wen@climate.gsfc.nasa.gov)

(Received October 25, 2000; revised February 12, 2001; accepted February 16, 2001.)